

# Statistical Modeling of Cardiovascular Signals and Parameter Estimation Based on the Extended Kalman Filter

James McNames, *Senior Member, IEEE*, and Mateo Aboy\*, *Member, IEEE*

**Abstract**—Cardiovascular signals such as arterial blood pressure (ABP), pulse oximetry (POX), and intracranial pressure (ICP) contain useful information such as heart rate, respiratory rate, and pulse pressure variation (PPV). We present a novel state-space model of cardiovascular signals and describe how it can be used with the extended Kalman filter (EKF) to simultaneously estimate and track many cardiovascular parameters of interest using a unified statistical approach. We analyze data from four databases containing cardiovascular signals and present representative examples intended to illustrate the versatility, accuracy, and robustness of the algorithm. Our results demonstrate the ability of the algorithm to estimate and track several clinically relevant features of cardiovascular signals. We illustrate how the algorithm can be used to elegantly solve several actively researched and clinically significant problems including heart and respiratory rate estimation, artifact removal, pulse morphology characterization, and PPV estimation.

**Index Terms**—Cardiovascular signals, extended Kalman filter (EKF), heart rate estimation, pulse pressure variation (PPV) estimation, respiratory rate estimation.

## I. INTRODUCTION

KALMAN filters and extended Kalman filters (EKF) have been extensively used to solve estimation and tracking problems involving electrocardiogram (ECG) and electroencephalogram (EEG) signals. For instance, Kalman filters have been used to solve estimation and processing problems on ECG signals such as the inverse problem of electrocardiography [1], intelligent ischemia monitoring [2], heart rate estimation [3], study and detection of cardiac arrhythmias [4], [5], model-based QRS delineation [6], and time-varying analysis of heart rate variability [7]. In EEG processing, the Kalman filter has been used to model EEG signals [8], address the problem of EEG segmentation [9], [10], for EEG noise-reduction [11], to study functional interactions within the newborn brain investigated by adaptive Kalman-based coherence analysis of

EEG [12], to solve the dynamical inverse problem of EEG generation using spatiotemporal Kalman filtering [13], analysis of the epileptic EEG [14], [15], and others [16]–[22]

Despite the success of the Kalman filter and model-based signal processing framework to solve relevant problems in ECG and EEG analysis, it has not been widely applied to solve estimation and tracking problems involving cardiovascular signals such as arterial blood pressure (ABP), intracranial pressure (ICP), and pulse oximetry (POX) [23]. The lack of its application to solve problems on cardiovascular pressure signals is due, in part, to the unavailability of statistical models for these signals which can be used within the Kalman filter framework.

Cardiovascular signals contain parameters of clinical significance that must be estimated, but have a complicated nonlinear relationship to the observed signals. For instance, accurate estimation and tracking of the heart and respiratory frequencies from ABP, POX, and ICP is important for algorithms embedded in patient monitors in the emergency room and intensive care applications. Commercial monitoring systems often include the capability to monitor heart rate and several statistics of pressure signals such as the systolic, diastolic, and mean, but few can reliably estimate other components of pressure waveforms such as the respiratory rate, pulse pressure variation (PPV), harmonic phases, or pulse morphology.

We propose a statistical state-space model of cardiovascular signals that is designed for use with EKF algorithms to estimate parameters of clinical interest such as the cardiac fundamental frequency and higher harmonics, respiratory fundamental frequency and higher harmonics, cardiac component harmonic amplitudes and phases, respiratory component harmonic amplitudes and phases, and PPV.

We use the EKF to estimate and track all the model parameters from arterial blood pressure (ABP) signals and illustrate its ability to solve five relevant problems on ABP, POX, and ICP analysis.

- 1) Estimation and tracking of heart rate from pressure signals.
- 2) Estimation and tracking of respiratory rate from pressure signals.
- 3) Model-based filtering, artifact removal, and interpolation.
- 4) Cardiovascular signal decomposition, characterization, and tracking of pulse morphology.
- 5) PPV estimation on mechanically ventilated subjects during periods of abrupt hemodynamic monitoring

These problems have important clinical significance. For instance, accurate estimation and tracking of PPV is important, since numerous studies have found that PPV is one of the

Manuscript received November 15, 2006; revised April 3, 2007. *Asterisk indicates corresponding author.*

J. McNames is with the Biomedical Signal Processing Laboratory and the Department of Electrical and Computer Engineering, Portland State University, Portland, OR 97201 USA (e-mail: mcnames@pdx.edu).

\*M. Aboy is with the Biomedical Signal Processing Laboratory, Portland State University, Portland, OR 97201 USA, and also with the Department of Electronics Engineering Technology, Oregon Institute of Technology, 18640 NW Walker Rd., Suite 2001, Beaverton, OR 97006 USA (e-mail: mateoaboy@ieee.org).

Color versions of one or more of the figures in this paper are available online at <http://ieeexplore.ieee.org>.

Digital Object Identifier 10.1109/TBME.2007.910648

most sensitive and specific predictors of fluid responsiveness, and PPV is used to optimize fluid therapy [24]–[29]. Characterization and tracking of the ICP pulse morphology during intracranial hypertension is also important. Several research studies have indicated ICP morphology changes correlate with a deterioration of the mechanisms that control ICP [30], [31], [31]–[34], and great interest exists in developing indices [31], [33]–[37] to characterize and track the pulse morphology in order to understand how such changes in morphology are related to intracranial compliance, cerebral autoregulation (CAR), and outcome. Accurate tracking of the heart rate and respiratory rate from cardiovascular signals without the need for an automatic beat detection algorithm is also important. The ability to track heart rate without performing beat detection is significant since there are currently few publicly available detection algorithms for cardiovascular pressure signals such as ABP, ICP, and POX [38]. Additionally, the EKF can be used as a preprocessing algorithm to estimate the heart and respiratory rate frequencies and to eliminate signal artifacts in order to greatly improve the accuracy of automatic detection algorithms [38]. Finally, biomedical signal models are important tools for development and validation of algorithms and systems that operate on physiological signals [39]. Most algorithms cannot be tested directly on data since the parameter of interest is not directly measurable [40]. Despite the fact that simple models for cardiovascular pressure signals have been extensively used in research for a variety of applications [23], [29], [41]–[43], currently there are no journal publications describing physiological pressure models.

## II. ALGORITHM DESIGN

The Kalman filter recursively estimates the state of a linear stochastic process such that the mean squared error is minimized. The extended Kalman filter (EKF) is a generalization that uses local linear approximations to continuously track the estimated state in nonlinear systems. In both cases, the state is estimated in a recursive manner that has modest storage and computational requirements.

In order to apply the EKF recursions, we must first express the relationship between the variables of interest and the observed signal in state space form

$$\mathbf{x}(n+1) = f[\mathbf{x}(n)] + \mathbf{u}(n) \quad (1)$$

$$\mathbf{y}(n) = h[\mathbf{x}(n)] + \mathbf{v}(n) \quad (2)$$

where  $\mathbf{x}(n)$  is a vector that represents the state of the system,  $\mathbf{u}(n)$  is the process noise with a covariance matrix  $Q$ ,  $\mathbf{y}(n)$  is a vector of the observed signals, and  $\mathbf{v}(n)$  is the observation or measurement noise with a variance of  $r$ . The first (1) is called the process or state model and (2) is called the measurement or observation model, and collectively these equations comprise the statistical state space model of the process. The most critical decision in adopting the EKF framework is to design these two models in a manner that incorporates known physiologic mechanisms and uses a compact state vector  $\mathbf{x}(n)$  that contains the variables of interest. We describe our proposed designs of these models in the following two sections.

### A. Observation Model

Our observation model of the cardiovascular signal consists of four primary components and is given by

$$y(n) = m(n) + y_r(n) + [1 + y_p(n)]y_c(n) + v(n) \quad (3)$$

where  $m(n)$  represents a low-frequency signal trend,  $y_r(n)$  is a quasi-periodic respiratory signal with a fundamental frequency equal to the respiratory rate,  $y_p(n)$  is another quasi-periodic signal due to respiration that causes an amplitude modulation of the cardiac component,  $y_c(n)$  is a quasi-periodic cardiac signal with a fundamental frequency equal to the heart rate, and  $v(n)$  is a white noise signal that accounts for the variation that is not explained by the other three components.

These four basic components are present in varying degrees in all of the cardiovascular signals that are currently monitored in clinical settings. Thus, the model is versatile enough to be applied to a wide variety of signals including cardiovascular pressure signals such as central venous pressure, arterial blood pressure, and intracranial pressure; the electrocardiogram; impedance plethysmography signals; and optical reflectance or transmittance signals commonly used in pulse oximetry.

In a hospital setting, patients are usually stationary and often sedated. In these cases, the respiratory and heart rates are quasi-periodic signals with slowly varying fundamental frequencies, amplitudes, and morphologies. Since any periodic signal can be represented as a sum of sinusoids, we modeled these signals as sums of sinusoids with slowly varying amplitudes, phases, and frequencies

$$y_c(n) = \sum_{k=1}^{N_c} a_c^2(k, n) \sin[k\theta_c(n) + \phi_c(k, n)] \quad (4)$$

$$y_r(n) = \sum_{k=1}^{N_r} a_r^2(k, n) \sin[k\theta_r(n) + \phi_r(k, n)] \quad (5)$$

where  $N_c$  and  $N_r$  are the number of harmonics for the cardiac and respiratory signals, respectively;  $a_c^2(k, n)$  and  $a_r^2(k, n)$  are the slowly varying amplitudes for the  $k$ th harmonic of the cardiac and respiratory signals;  $\theta_c(n)$  and  $\theta_r(n)$  are the instantaneous cardiac and respiratory phases; and  $\phi_c(k, n)$  and  $\phi_r(k, n)$  are the slowly varying phases of the cardiac and respiratory signals. Similar models have been used in pitch tracking for speech signals.

In this model, the user specifies the number of harmonics for the respiratory and cardiac signals. Generally, a large number of harmonics are necessary to accurately model the signal when sharp features are present in the signal, such as the QRS complex in an ECG signal. When the signal is smooth and nearly sinusoidal, such as the respiratory component of cardiovascular pressure signals, only a few harmonics are necessary. In general, the number of harmonics can be selected based on a spectral analysis of a representative sample of the signals of interest.

Respiratory fluctuations are known to affect most cardiovascular signals in three different ways. First, there is generally an additive respiratory component, which we model as  $y_r(n)$ . Second, there is often an amplitude modulation (AM), which is sometimes called pulse pressure variation or pulsus paradoxus, under pathologic conditions. The amplitude modulation can be

caused by the effect of respiration on venous preload during the cardiac cycle and expansion of the arterial tree. We model this effect as an amplitude modulation of the cardiac component  $y_c(n)$  in (3), which is related to the additive component through a finite-impulse response (FIR) filter

$$y_p(n) = \sum_{\ell=0}^{N_h-1} h_p(\ell, n) y_r(n - \ell) \quad (6)$$

where  $N_h$  is the number of filter coefficients specified by the user. The purpose of the FIR filter is to account for the changes in amplitudes, phases, and delay between the additive and amplitude modulation components of respiration, while maintaining the same slowly changing fundamental frequency. Third, the respiratory component affects the heart rate through several mechanisms including vagal nerve inhibition and the baroreflex loop. We model this frequency modulation of the heart rate, which is often called respiratory sinus arrhythmia, as a frequency modulation of the heart rate. This is described in greater detail in the following section.

### B. State Model

Our state vector  $\mathbf{x}(n)$  includes all of the unknown parameters of clinical significance

$$\mathbf{x}(n) \triangleq \begin{bmatrix} m(n) \\ \omega_{ca}(n) \\ \theta_c(n) \\ \{a_c(k_c, n)\} \\ \{\phi_c(k_c, n)\} \\ \omega_r(n) \\ \theta_r(n) \\ \{\theta_r(n - \ell)\} \\ \{a_r(k_r, n)\} \\ \{a_r(k_r, n - \ell)\} \\ \{\phi_r(k_r, n)\} \\ \{\phi_r(k_r, n - \ell)\} \\ \{h_p(\ell, n)\} \\ \{h_f(\ell, n)\} \end{bmatrix} \quad \text{for} \quad \begin{array}{l} k_r = 1, \dots, N_r \\ k_c = 1, \dots, N_c \\ \ell = 1, \dots, N_{h-1} \end{array} \quad (7)$$

The elements of the state vector are defined in Table I. Our state model is given by (1) where

$$f[\mathbf{x}(n)] = \begin{bmatrix} m(n) \\ \bar{\omega}_c + \alpha_c \{s_c [\omega_{ca}(n)] - \bar{\omega}_c\} \\ \theta_c(n) + T_s s_c [\omega_{cr}(n) + \omega_{ca}(n)] \\ \{a_c(k_c, n)\} \\ \{\phi_c(k_c, n)\} \\ \bar{\omega}_r + \alpha_r \{s_r [\omega_r(n)] - \bar{\omega}_r\} \\ \theta_r(n) + T_s s_r [\omega_r(n)] \\ \{\theta_r(n + 1 - \ell)\} \\ a_r(k_r, n) \\ \{a_r(k_r, n + 1 - \ell)\} \\ \phi_r(k_r, n) \\ \{\phi_r(k_r, n - \ell)\} \\ \{h_p(\ell, n)\} \\ \{h_f(\ell, n)\} \end{bmatrix} \quad (8)$$

TABLE I  
LIST OF ALL MODEL PARAMETERS AND THEIR INITIAL VALUES

Name	Symbol	Number	Initial
Signal Trend	$m(n)$	1	$y(0)$
Cardiac frequency (non-respiratory)	$\omega_{ca}(n)$	1	$\bar{\omega}_c$
Cardiac Phase	$\theta_c(n)$	1	0
Cardiac Harmonic Amplitudes	$a_{c,k}(n)$	$N_c$	Varies
Cardiac Harmonic Phases	$\phi_{c,k}(n)$	$N_c$	0
Respiratory Frequency	$\omega_r(n)$	1	$\bar{\omega}_r$
Respiratory Phase	$\theta_r(n - \ell)$	1	0
Respiratory Harmonic Amplitudes	$a_{r,k}(n - \ell)$	$N_r$	Varies
Respiratory Harmonic Phases	$\phi_{r,k}(n - \ell)$	$N_r$	0
Amplitude modulation filter coefficients	$h_p(\ell, n)$	$N_h$	0
Frequency modulation filter coefficients	$h_f(\ell, n)$	$N_h$	0

$$\mathbf{u}(n) = \begin{bmatrix} u_m(n) \\ u_{\omega_{ca}}(n) \\ 0 \\ \{u_{a_c}(k_c, n + 1)\} \\ \{u_{\phi_c}(k_c, n + 1)\} \\ u_{\omega_r}(n) \\ 0 \\ \{0\} \\ u_{a_r}(n) \\ \{0\} \\ u_{\phi_r}(n) \\ \{0\} \\ \{u_{h_p}(\ell, n + 1)\} \\ \{u_{h_f}(\ell, n + 1)\} \end{bmatrix} \cdot \quad (9)$$

The state model includes past values of the respiratory frequency, amplitudes, and phases for use in the FIR filters that are used to model the amplitude modulation and frequency modulation components of the respiratory variation.

Most of the remaining state variables are modeled as a random walk where the variance, or average step size, is controlled by the variance of the corresponding process noise term in the vector  $\mathbf{u}(n)$ , which are collectively represented in the covariance matrix  $Q$ . This is a common statistical model in adaptive filter applications when the parameters of interest are known to drift slowly over time, but an explicit statistical model based on domain knowledge is unavailable [44].

The random walk noise variances determine the tradeoff between the bias and variance of the estimates. If the noise variance for a parameter is small, the estimated value will be less sensitive to the observed signal  $y(n)$ , will change more slowly over time, and may not be able to track rapid fluctuations. If the noise variance for a parameter is large, the estimated value will be more sensitive to  $y(n)$ , may contain excessive variation, and will be able to track rapid fluctuations. The tradeoff between these two extremes must be made by a careful selection of the noise variance by the user.

1) *Instantaneous Phase State Model*: The cardiac and respiratory instantaneous phases do not use a random walk model. If we assume that the phase components of the cardiac and respiratory harmonics,  $\phi_c(k, n)$  and  $\phi_r(k, n)$ , are slowly varying, then the instantaneous respiratory and cardiac frequencies are given by

$$\omega(n) \triangleq \frac{d\theta(n)}{dn} \approx \frac{\theta(n + 1) - \theta(n)}{T_s} \quad (10)$$

where  $T_s = f_s^{-1}$  is the sampling interval. This leads us to use the first-order difference equation as our state model for the instantaneous phases

$$\theta(n+1) = \theta(n) + T_s s[\omega(n)] \quad (11)$$

where  $\omega(n)$  is the instantaneous frequency in units of radians per sample, and  $s[\omega]$  is a saturation function that limits the range of the instantaneous frequency to known physiologic limits. We used a simple clipping function

$$s[\omega] = \begin{cases} \omega_{\min} & \omega < \omega_{\min} \\ \omega & \omega_{\min} \leq \omega \leq \omega_{\max} \\ \omega_{\max} & \omega_{\max} \leq \omega \end{cases} . \quad (12)$$

The generalization to softer saturation functions is straightforward. The use of this function improves the stability of the tracking algorithm and its robustness to common types of artifact.

2) *Respiratory Sinus Arrhythmia*: The cardiac frequency is composed of two components

$$\omega_c(n) = \omega_{cr}(n) + \omega_{ca}(n) \quad (13)$$

where  $\omega_{cr}(n)$  models the frequency modulation (FM) of the heart rate due to respiration, which is often called the respiratory sinus arrhythmia (RSA) or high-frequency component of the heart rate variability (HRV). The second term  $\omega_{ca}(n)$  models the remaining heart rate variability. In the same manner as we modeled the amplitude modulation, the FM of the heart rate is related to the additive respiratory component through an FIR filter

$$\omega_{cr}(n) = \sum_{\ell=0}^{N_h-1} h_f(\ell, n) y_r(n-\ell) \quad (14)$$

where  $N_h$  is the number of filter coefficients specified by the user. As with the AM component, the FIR filter accounts for the changes in amplitudes, phases, and delay between the additive and FM components of respiration, while maintaining the same slowly changing fundamental frequency.

3) *Respiratory and Heart Rate State Models*: The fluctuations in the respiratory rate  $\omega_r(n)$  and fluctuations in the heart rate  $\omega_{ca}(n)$  that are not due to RSA are both modeled as a first-order autoregressive process with a mean and mild nonlinearity that limit the frequencies to known physiologic ranges

$$\omega_r(n+1) = \bar{\omega}_r + \alpha_r \{s_r[\omega_r(n)] - \bar{\omega}_r\} + u_{\omega_r}(n) \quad (15)$$

$$\omega_{ca}(n+1) = \bar{\omega}_c + \alpha_c \{s_c[\omega_{ca}(n)] - \bar{\omega}_c\} + u_{\omega_{ca}}(n) \quad (16)$$

where  $\bar{\omega}_r$  and  $\bar{\omega}_c$  are the *a priori* estimates of the expected respiratory and cardiac frequencies, respectively;  $\alpha_r$  and  $\alpha_c$  control the bandwidth of the frequency fluctuations; and  $u_{\omega_r}(n)$  and  $u_{\omega_{ca}}(n)$  are white noise processes that model the random variation in the respiratory and cardiac frequencies, respectively.

The instantaneous respiratory and heart rates in units of Hz are then

$$f_r(n) = \frac{1}{2\pi T_s} s_r[\omega_r(n)] \quad (17)$$

$$f_c(n) = \frac{1}{2\pi T_s} s_c[\omega_c(n)] . \quad (18)$$

### C. State Estimation

The extended Kalman filter is based on a local linear approximation of the state-space model about an estimate of the state. Other generalizations of the Kalman filter recursions to nonlinear state space models have been developed such as the unscented Kalman filter [45] and particle filters, which could also be applied to this model [46].

Typically the linearization is only performed during the filter portion of the algorithm. The output is linearized about the predicted estimate  $\hat{\mathbf{x}}(n|n-1)$ , a prediction of the state at time  $n$  given only the preceding observations  $\{\mathbf{y}(n-1), \dots, \mathbf{y}(0)\}$ . The state prediction equation is linearized about the filtered estimate  $\hat{\mathbf{x}}(n|n)$ , an estimate of the state given the current and preceding observations  $\{\mathbf{y}(n), \dots, \mathbf{y}(0)\}$ . The extended Kalman filter recursions are as follows:

$$\begin{aligned} H_n &= J_{\mathbf{x}} h(\mathbf{x})|_{\mathbf{x}=\hat{\mathbf{x}}(n|n-1)} \\ r_{e,n} &= H_n P_{n|n-1} H_n^T + r \\ K_n &= P_{n|n-1} H_n^T r_{e,n}^{-1} \\ e(n) &= y(n) - h[\hat{\mathbf{x}}(n|n-1)] \\ \hat{\mathbf{x}}(n|n) &= \hat{\mathbf{x}}(n|n-1) + K_n e(n) \\ \hat{\mathbf{x}}(n+1|n) &= f[\hat{\mathbf{x}}(n|n)] \\ F_n &= J_{\mathbf{x}} f(\mathbf{x})|_{\mathbf{x}=\hat{\mathbf{x}}(n|n)} \\ P_{n|n} &= (I - K_n H_n) P_{n|n-1} \\ P_{n+1|n} &= F_n P_{n|n} F_n^T + Q \end{aligned}$$

where  $J_{\mathbf{x}}$  denotes the Jacobian operator.

To further improve robustness of the frequency estimates, the innovations  $e(n)$  were included in the clipping functions for the instantaneous phase updates to help improve stability and robustness of the algorithm

$$\hat{\theta}(n+1|n) = \theta(n|n-1) + T_s s \left[ \hat{\omega}(n|n) + \frac{1}{T_s} K_{n,\theta} e(n) \right] \quad (19)$$

where  $K_{n,\theta}$  is the element of the Kalman gain vector corresponding to  $\theta(n)$ . This ensures that the instantaneous frequency, defined by (10), never exceeds the physiologic limits specified by the user.

The algorithm requires an initial estimate of the state vector  $\hat{\mathbf{x}}(0|-1)$  and the initial state covariance matrix  $P_{0|-1}$ . The initial values of the estimated state are listed in Table I. The initial state covariance was a diagonal matrix with 1% of the variance values listed in Table II.

### D. User-Specified Parameters

All the variables included as part of our statistical model for cardiovascular signals have a clear physiologic interpretation. Much is known about the character and range of these variables that can be used to improve the performance of the estimator. The state space modeling framework provides the means to elegantly use this type of domain knowledge to improve the estimation accuracy and tracking. Table II lists all of the user-specified parameters. The values listed in this table are those used for the first application example described later.

TABLE II  
USER-SPECIFIED MODEL PARAMETERS

Name	Symbol	Value
Cardiac minimum frequency	$f_{c,\min}$	1.000 Hz
Cardiac mean frequency	$f_c$	1.400 Hz
Cardiac maximum frequency	$f_{c,\max}$	2.000 Hz
Cardiac cutoff frequency	$f_{c,\text{co}}$	0.001 Hz
Cardiac harmonics	$N_c$	6
Cardiac frequency variance	$\sigma_{\omega_c}^2$	0.050 Hz
Cardiac harmonic amplitude variance	$\sigma_{a_c}^2$	0.000 mmHg <sup>2</sup>
Cardiac harmonic phase variance	$\sigma_{\phi_c}^2$	0.000 rad <sup>2</sup>
Respiratory minimum frequency	$f_{r,\min}$	0.150 Hz
Respiratory mean frequency	$f_r$	0.250 Hz
Respiratory maximum frequency	$f_{r,\max}$	0.400 Hz
Respiratory cutoff frequency	$f_{r,\text{co}}$	0.001 Hz
Respiratory harmonics	$N_r$	2
Respiratory frequency variance	$\sigma_{\omega_r}^2$	0.050 Hz
Respiratory harmonic amplitude variance	$\sigma_{a_r}^2$	0.000 mmHg <sup>2</sup>
Respiratory harmonic phase variance	$\sigma_{\phi_r}^2$	0.000 rad <sup>2</sup>
Trend variance	$\sigma_m^2$	0.500 mmHg <sup>2</sup>
Filter length		10
Filter variance AM		0.000
Filter variance FM		0.000
Measurement noise variance		30.000 mmHg <sup>2</sup>

### E. Pulse Pressure Variation (PPV)

PPV quantifies the degree of variation in the pulsatile amplitude of arterial blood pressure signals due to respiration. It is a form of amplitude modulation of the pressure waveform caused by intrathoracic pressure fluctuations that occur with respiration. The standard method for calculating  $\Delta\text{PP}$  often requires simultaneous recording of arterial and airway pressure. Pulse pressure (PP) is calculated on a beat-to-beat basis as the difference between systolic and diastolic arterial pressure. Maximal PP ( $\text{PP}_{\max}$ ) and minimal PP ( $\text{PP}_{\min}$ ) are calculated over a single respiratory cycle, which is determined from the airway pressure signal. Pulse pressure variations  $\Delta\text{PP}$  are calculated in terms of  $\text{PP}_{\max}$  and  $\text{PP}_{\min}$  and expressed as a percentage

$$\Delta\text{PP}(\%) = 100 \times \frac{\text{PP}_{\max} - \text{PP}_{\min}}{\frac{(\text{PP}_{\max} + \text{PP}_{\min})}{2}}. \quad (20)$$

The variation in the pulse pressure can also be quantified by the coefficient of variation (CV) of the pulse pressure

$$\text{CV} \triangleq \frac{\sigma_{\text{PP}}}{\mu_{\text{PP}}}. \quad (21)$$

The CV can be estimated from our statistical model as the standard deviation of  $y_p(n)$ ,  $\text{CV} = \sigma_{y_p}(n)$ . Since  $y_p(n)$  is the output of a linear time-varying filter with a quasi-periodic input signal, the power of  $y_p(n)$  can be estimated as

$$\sigma_{y_p}^2(n) = \frac{1}{2} \sum_{k=1}^{N_r} a_r^4(k, n) \left| H_p \left( e^{jk\omega_r(n)}, n \right) \right|^2 \quad (22)$$

where  $H_p \left( e^{jk\omega_r(n)}, n \right)$  is the frequency response of the time-varying filter

$$H_p \left( e^{jk\omega_r(n)}, n \right) = \sum_{\ell=0}^{N_h-1} h_p(\ell, n) e^{-jk\omega_r(n)\ell}. \quad (23)$$

## III. RESULTS AND DISCUSSION

In this section, we demonstrate versatility and utility of our proposed statistical model for cardiovascular signals and the EKF estimator in four applications. In each case, the EKF is used to estimate and track model parameters in various cardiovascular signals.

- 1) Arterial blood pressure (ABP) signals. This illustrates its ability to solve three relevant problems in ABP analysis: 1) estimation and tracking of heart rate on pressure signals, 2) estimation and tracking of the respiratory rate from pressure signals, and 3) model-based filtering, artifact removal, and interpolation.
- 2) Pulse oximetry (POX) signals. This illustrates its ability to solve the problem of heart and respiratory rate estimation from POX.
- 3) Intracranial pressure (ICP) signals. This illustrates its ability to solve the problem of ICP pulse morphology estimation and tracking during periods of intracranial hypertension.
- 4) Pressure signals with pulse pressure variation (PPV). This illustrates its ability to solve the problem of PPV estimation and tracking on mechanically ventilated subjects.

### A. Data

1) *ABP and POX Database*: The MIMIC database and Massachusetts General Hospital/Marquette Foundation (MGH/MF) Waveform Database [47] (Physionet) [48] were used to assess the ability of the proposed EKF to estimate and track all the model parameters of clinical interest from ABP and POX signals. The database consists of long-term recordings of cardiovascular signals (e.g., ECG, ABP, POX, and impedance plethysmography) recorded in an intensive care setting from a patient monitor. All of the signals were sampled at 125 Hz, except the electrocardiogram, which was sampled at 500 Hz. Derived parameters such as the heart rate and respiratory rate were sampled at 0.977 Hz.

2) *ICP Database*: The database used to evaluate the ability of the EKF to estimate and track all the model parameters from ICP signals and to demonstrate the algorithm usefulness as a tool to characterize the ICP pulsatile morphology included 63 ICP signals from patients with significant head injuries who were admitted to the pediatric intensive care unit at the Doernbecher Children's Hospital. ICP was monitored continuously using a ventricular catheter or parenchymal fiber-optic pressure transducer (Integra NeuroCare, Integra LifeSciences, Plainsboro, NJ). The ICP monitor was connected to a Philips Merlin CMS patient monitor (Philips, Best, The Netherlands) that sampled the ICP signals at 125 Hz. An HPUX workstation automatically acquired these signals through a serial data network, and they were stored in files on CD-ROM [49]. Patients were managed according to the standards of care in pediatric intensive care unit at Doernbecher Children's Hospital. The data acquisition protocol was reviewed and approved by the Institutional Review Board at Oregon Health and Science University (OHSU), and the requirement of informed consent was waived.

3) *PPV Database*: The database used to evaluate the ability of the EKF to estimate PPV contained ABP signals sampled at 50 Hz obtained from 18 mechanically ventilated crossbred Yorkshire swine for a total of over 40 h of ABP recordings. These recordings were acquired at an animal laboratory at OHSU. The subjects underwent Grade V liver injury after splenectomy while receiving mechanical ventilation and general anesthesia with isoflurane. The severe blood loss resulted in hemorrhagic shock, followed by fluid resuscitation with either 0.9% normal saline or lactated ringers solutions. Trained experts manually calculated PPV at five time instances during the period of abrupt hemodynamic changes. These expert manual annotations provide a “gold standard” for algorithm comparison and validation. The study protocol was reviewed and approved by the Institutional Review Board at OHSU.

### B. Heart and Respiratory Rate Estimation and Interpolation of ABP

The following application example illustrates the results obtained with the EKF on a representative ABP signal selected from the MIMIC database, and the ability of the proposed EKF to solve three relevant problems on ABP analysis: 1) estimation and tracking of heart rate on pressure signals, 2) estimation and tracking of the respiratory rate from pressure signals, and 3) model-based filtering, artifact removal, and interpolation. The cardiovascular signal for this example was obtained from patient record number 240 starting 50 min into the record. This was obtained from a 68 year old male patient with angina. Fig. 1(a) shows a spectrogram of the ABP signal with the cardiac frequency estimated by the EKF overlaid (white line), and Fig. 1(b) shows the corresponding spectrogram of the residuals using the same color scale. The spectrogram was estimated using a modified periodogram with a 20 s Blackman window [50]. The signal spectrogram demonstrates that the EKF can track the heart rate shown by the horizontal bands at harmonic frequencies of the heart rate ranging from 1.2–1.5 Hz. The effects of respiration can also be seen in this figure. The additive component can be seen as the horizontal band ranging from 0.2–0.3 Hz. The amplitude and frequency modulation effects can be seen as sidebands about the cardiac component. The residual spectrogram shows that there is relatively little power left at these frequencies, which demonstrates that the EKF is able to explain the systematic variation of most of these components.

Fig. 1(e) shows the heart rate as estimated by an algorithm in the patient monitor from the electrocardiogram and the estimate produced by the EKF from the pressure signal. These estimates are nearly identical, and the estimate produced by the EKF precedes the estimate from the patient monitor by approximately 5 s.

Fig. 1(c) shows the estimated respiratory rate overlaid on top of the spectrogram (white line). The spectrogram was estimated using a modified periodogram with a 40 s Blackman window [50]. The second harmonic is quite faint in this case, but the EKF is able to track the respiratory rate accurately throughout most of the signal. Note that the EKF initially has difficulty locking onto the respiratory component but is able to

track rapid respiratory fluctuations starting at approximately 100 s into the recording. The respiratory component appears to bifurcate at 160 s and becomes clear again at 220 s. The EKF is able to regain track quickly shortly after this event, at approximately 240 s. This demonstrates the robustness of the algorithm and the ability to regain track quickly. Automatic estimation of the respiratory rate from cardiovascular signals is an important and difficult problem. Classical techniques involving heuristic algorithms that find frequency corresponding to the maximum power spectral density over a user-specified range often fail during abrupt edges since the power at the low frequencies corrupts the spectrum at the respiratory frequency.

Fig. 1(f) shows an example of the EKF applied to an ABP signal during a premature ventricular contraction (PVC). This recording was obtained from the MGH/MF Waveform Database. The predicted signal values estimated by the EKF contain an estimate what the normal morphology might have been if the PVC had not occurred. This demonstrates the ability of the EKF to interpolate entire cardiovascular signal pulsatile components during regions of artifact or clinical abnormalities. The ability of the EKF to perform model-based signal processing in order to filter out noise and artifact that are inconsistent with the statistical model of the observed cardiovascular pressure signal is a critical preprocessing task required to solve many other practical problems of biosignal analysis.

This example demonstrates the ability of the EKF to accurately track the heart rate and respiratory rate in pressure signals without the need for automatic beat detection algorithm. The ability to track heart rate without performing beat detection is significant since there are currently few publicly available detection algorithms for cardiovascular pressure signals such as ABP, ICP, and POX [38]. Additionally, the EKF can be used as a preprocessing algorithm to estimate the heart and respiratory rate frequencies and to eliminate signal artifact, which improves the accuracy of automatic detection algorithms [38].

### C. Estimation and Tracking of Respiratory Rate From POX

The following application example demonstrates how well the EKF can track the parameters of interest, such as the heart and respiratory rates, using only an infrared absorption signal used in pulse oximetry (POX). The signal was selected from the MIMIC database.

Fig. 2 shows four estimates of the respiratory rate. All three of the plots show an estimate of the respiratory rate based on manual annotations as a thick, grey line to serve as a basis of comparison. The annotations were created based on a visual inspection of the respiratory transthoracic impedance plethysmography signal, which was measured from the lead I ECG electrodes. Fig. 2(a) shows the respiratory rate estimated by the patient monitor from this signal. Fig. 2(b) shows the respiratory rate estimated by the EKF from the ABP signal, and Fig. 2(c) shows the respiratory rate estimated from the EKF from the infrared signal acquired from a noninvasive pulse oximeter [51]. The EKF is able to track the respiratory rate more accurately from the ABP signal than the patient monitor is able to track it from the impedance plethysmography signal. The estimate from the POX signal is less accurate and takes longer to begin

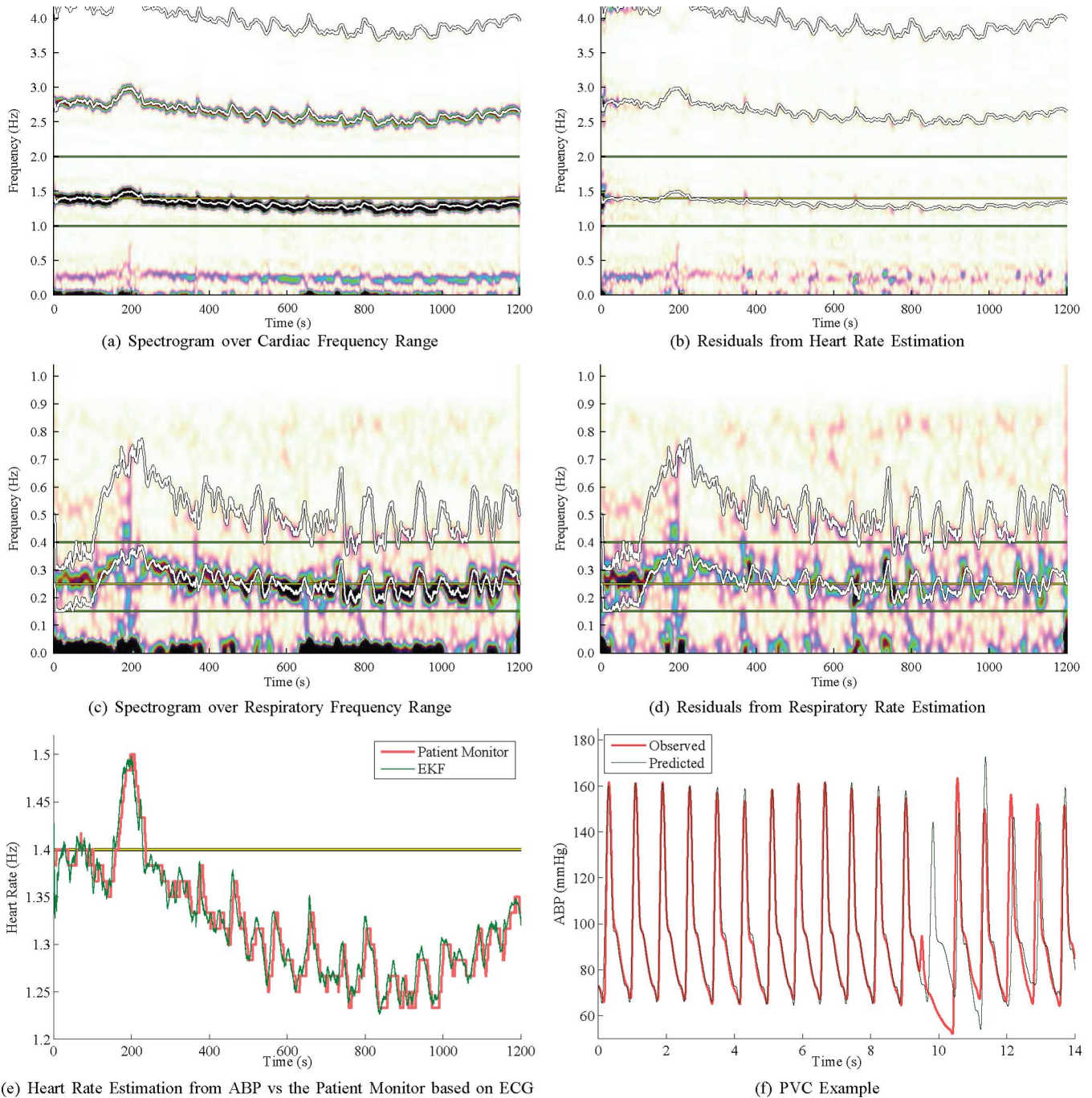


Fig. 1. Spectrogram of the ABP signal (a) and residuals (b) over a frequency range that shows the first three harmonics of the heart rate (a,b). The horizontal line at 1.5 Hz shows the mean cardiac frequency used by the EKF. The EKF estimate of the heart rate at the first three harmonics is overlaid as a white line on top of the spectrograms. Spectrogram of the ABP signal (c) and residuals (d) over a frequency range that shows the first two harmonics of the respiratory rate (c,d). The horizontal lines at 0.15, 0.25, and 0.40 Hz show the minimum, mean, and maximum respiratory frequencies used by the EKF. The EKF estimate of the respiratory rate at the first two harmonics is overlaid as a white line on top of the spectrograms. (e) Estimates of the heart rate by the patient monitor from the electrocardiogram (thick, light line) and by the EKF from the pressure signal (thin, dark line). (f) Example of the EKF tracking during a PVC.

tracking. This is partly due to the artifact in the POX signal and weaker respiratory components in this signal.

#### D. Tracking Changes in Pulsatile Morphology in ICP

In this example, we demonstrate the ability of the EKF to track pulsatile morphology changes in ICP during a period of intracranial hypertension. Traumatic brain injury (TBI) is a leading cause of death and disability in the U.S. [52]. Elevated intracranial pressure often results in secondary injury due to

decreased cerebral perfusion pressure and cerebral ischemia [32], [53]. It is generally accepted that continuous monitoring of ICP signals has resulted in improved patient outcome [33]. Current ICP therapy is based predominantly on the mean ICP and the ICP pulse morphology. Generally, clinicians intervene to lower mean ICP when it exceeds a threshold, which is usually 20 mmHg [54]. Taken alone, the mean ICP does not indicate the source of hypertension, such as poor brain compliance or impaired cerebral autoregulation (CAR) [31],

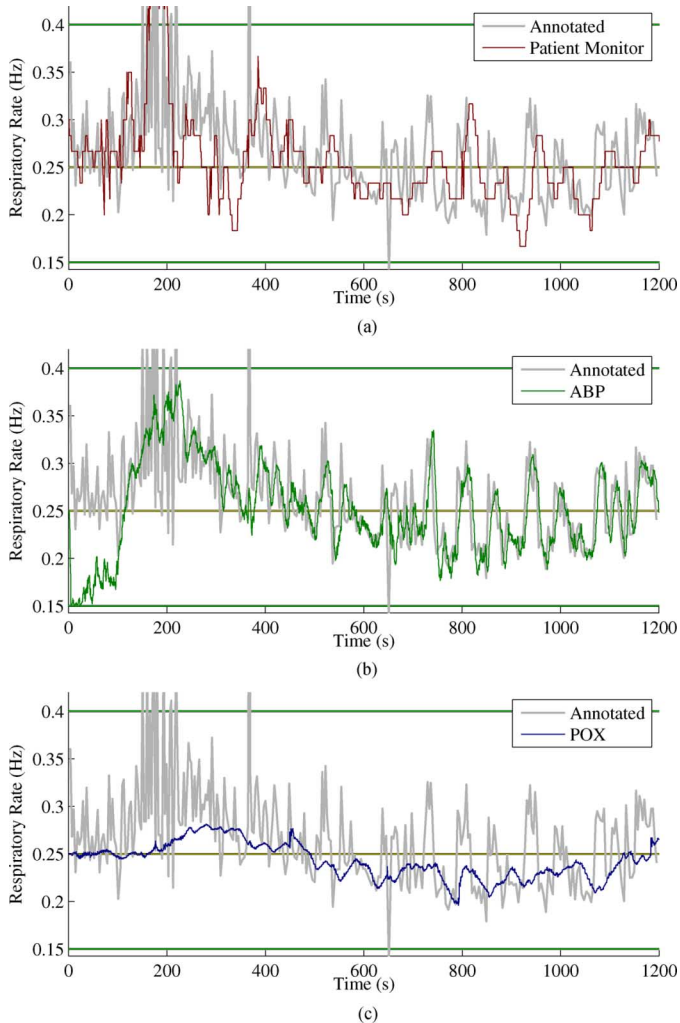


Fig. 2. Estimates of the respiratory rate by manual annotations of the impedance signal acquired from the ECG leads, by the patient monitor from the ECG impedance, by the EKF from the ABP signal, and by the EKF from the POX signal. The horizontal lines at 0.15, 0.25, and 0.40 Hz show the minimum, mean, and maximum respiratory frequencies used by the EKF. (a) Patient Monitor. (b) Estimate from ABP. (c) Estimate from POX.

[55]. Determining ways to better understand and track these variables remains a significant research goal.

It is generally accepted that the ICP pulse morphology is associated with mean ICP, brain compliance, and CAR. As mean ICP increases, compliance decreases, and CAR becomes impaired, the pulse morphology is thought to undergo a “rounding” transition [30]–[32]. Several researchers have developed indices related to these variables that were derived from the ICP pulse morphology [31], [33], [34], [41], [55], [56]. These indices use methods such as spectral analysis [35],[36] and pulse slope [37] to quantify the ICP pulse morphology.

The proposed EKF provides a solution to the problem of ICP pulse morphology characterization by providing the ability to estimate and track a set of parameters that can be used to characterize the ICP pulse morphology. Fig. 3 shows an example of the EKF applied to an intracranial pressure (ICP) signal acquired from an 11.5-year-old male with traumatic brain injury who was admitted to Doernbecher Children’s Hospital (ICP Database). The ICP signal was sampled at 125 Hz [49]. The three brief (5 s) segments shown in the top middle plot illustrate three

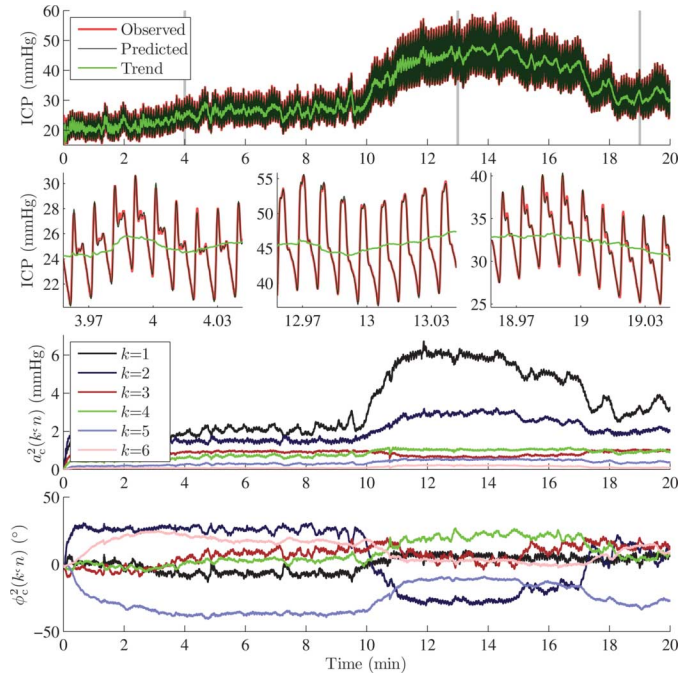


Fig. 3. Example of the EKF tracking changes in the pulsatile morphology of an intracranial pressure (ICP) signal during an episode of intracranial hypertension. The top plot shows the observed signal, predicted signal, and trend over a 20 min interval. The three top middle plots show short segments with three distinct types of ICP morphology. The times of these segments are shown by the vertical grey lines in the top plot. The bottom plots show the amplitude and phase components of the signal.

well-known changes in pulse morphology that are indicators of cerebral autoregulation and blood volume [30], [55], [57]. The bottom two plots illustrate how the EKF can be used to continuously track changes in amplitude and phase of the cardiac components that account for the pulse morphology. The characterization of these signal components as a compact set of metrics is a key advantage of the state space model. These components can be used to analyze and detect changes in the pulse morphology that are not easily discerned through a time domain plot or time–frequency analysis [58]. In this example, we can see that as the ICP mean increases the amplitudes of the first and second cardiac harmonics increase, while all the higher harmonics stay relatively constant. More significantly, the phase relationship between the harmonics changes considerably during the period of intracranial hypertension resulting in a rounding of the pulse morphology. The proposed statistical model and the EKF can be used to estimate and track the amplitude and phase relationship between all of the relevant harmonics in order to investigate ICP pulse morphology changes. Additionally, the EKF also track the heart rate, respiratory rate, respiratory effects on ICP, and all the other model parameters using a unified approach. The ability to estimate and track all the model parameters simultaneously using a single algorithm enables researchers to investigate the relationship of these parameters as a function of the mean ICP and pulse morphology.

#### E. Tracking Pulse Pressure Variation (PPV)

Numerous studies have found that pulse pressure variation (PPV) is one of the most sensitive and specific predictors of fluid responsiveness and is used to guide fluid therapy in multiple

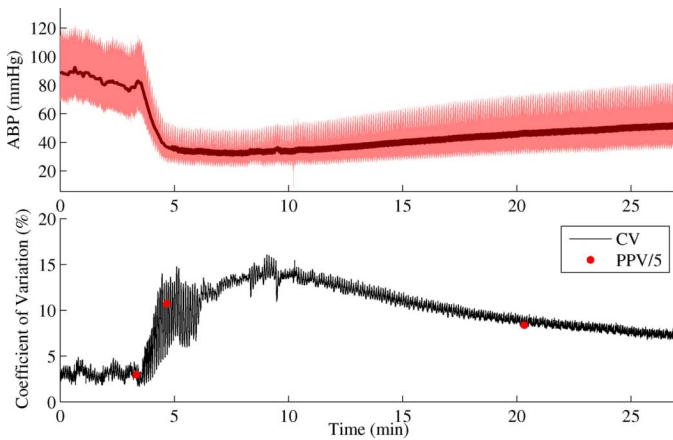


Fig. 4. Example of the EKF tracking pulse pressure variation (PPV) during a period of abrupt hemodynamic changes after an acute injury involving severe blood loss. The PPV estimated using the EKF (bottom plot, black) closely matches the expert annotations (dots).

patient populations receiving mechanical ventilation [24]–[28]. Currently, there are few publicly available algorithms capable of estimating PPV [29]. Thus, researchers need to rely on commercial devices such as the PiCCO system (Pulsion Medical Systems, Munich, Germany), which use proprietary algorithms for PPV estimation. The results of a recent study suggested that the PiCCO PPV algorithm may not work well in certain situations [59]. Our validation results indicate that the PiCCO system may not work well during regions of abrupt hemodynamic changes, such as in the example presented here to illustrate the EKF capability [60].

Fig. 4 shows an example illustrating the ability of the EKF algorithm to estimate and track variations in PPV during a period of significant hemodynamic changes. Note how the PPV estimates obtained with the EKF algorithm are consistent with the PPV expert annotations.

#### IV. CONCLUSION

We proposed a novel statistical state space model for cardiovascular signals such as ABP, POX, and ICP that can be used with the generalizations of the Kalman filter for nonlinear state space models, such as the EKF. The algorithm is able to decompose cardiovascular signals into clinically meaningful components and track them continuously.

We analyzed data from four databases containing cardiovascular signals and presented representative examples intended to illustrate the versatility, accuracy, and robustness of the algorithm to solve several significant problems. Specifically, we presented the results of applying the proposed algorithm to four representative signals corresponding to each of the four databases analyzed. These examples demonstrate that the algorithm can elegantly and accurately solve several well-defined and actively researched clinically significant problems. We emphasize that in this paper we have only *exemplified* how the proposed approach can be used to solve these problems. A complete scientific assessment study of the algorithm as a solution for each of these problems and a performance comparison against the best current practices must be conducted in order to fully assess its capabilities.

#### REFERENCES

- [1] K. L. Berrier, D. C. Sorensen, and D. S. Khoury, "Solving the inverse problem of electrocardiography using a Duncan and Horn formulation of the Kalman filter," *IEEE Trans Biomed. Eng.*, vol. 51, no. 3, pp. 507–515, Mar. 2004.
- [2] A. Bosnjak, G. Bevilacqua, G. Passariello, F. Mora, B. Sansó, and G. Carrault, "An approach to intelligent ischaemia monitoring," *Med. Biol. Eng. Comput.*, vol. 33, no. 6, pp. 749–756, Nov. 1995.
- [3] M. H. Ebrahim, J. M. Feldman, and I. Bar-Kana, "A robust sensor fusion method for heart rate estimation," *J. Clin. Monit.*, vol. 13, no. 6, pp. 385–393, Nov. 1997.
- [4] M. S. Woolfson, "Study of cardiac arrhythmia using the Kalman filter," *Med. Biol. Eng. Comput.*, vol. 29, no. 4, pp. 398–405, Jul. 1991.
- [5] D. F. Sittig and K. H. Cheung, "A parallel implementation of a multi-state Kalman filtering algorithm to detect EEG arrhythmias," *Int. J. Clin. Monit. Comput.*, vol. 9, no. 1, pp. 13–22, 1992.
- [6] L. Sörnmo, "A model-based approach to QRS delineation," *Comput. Biomed. Res.*, vol. 20, no. 6, pp. 526–542, Dec. 1987.
- [7] M. P. Tarvainen, S. D. Georgiadis, P. O. Ranta-Aho, and P. A. Karjalainen, "Time-varying analysis of heart rate variability signals with a Kalman smoother algorithm," *Physiol. Meas.*, vol. 27, no. 3, pp. 225–239, Mar. 2006.
- [8] M. Arnold, W. H. Miltner, H. Witte, R. Bauer, and C. Braun, "Adaptive ar modeling of nonstationary time series by means of Kalman filtering," *IEEE Trans. Biomed. Eng.*, vol. 45, no. 5, pp. 553–562, May 1998.
- [9] J. S. Barlow, "Methods of analysis of nonstationary EEGs, with emphasis on segmentation techniques: A comparative review," *J. Clin. Neurophysiol.*, vol. 2, no. 3, pp. 267–304, Jul. 1985.
- [10] A. Hasman, B. H. Jansen, G. H. Landeweerd, and A. W. van Blokland-Vogelansang, "Demonstration of segmentation techniques for EEG records," *Int. J. Biomed. Comput.*, vol. 9, no. 4, pp. 311–321, Jul. 1978.
- [11] F. Bartoli and S. Cerutti, "An optimal linear filter for the reduction of noise superimposed to the EEG signal," *J. Biomed. Eng.*, vol. 5, no. 4, pp. 274–280, Oct. 1983.
- [12] M. Eiselt, J. Schindler, M. Arnold, H. Witte, U. Zwiener, and J. Frenzel, "Functional interactions within the newborn brain investigated by adaptive coherence analysis of EEG," *Neurophysiol. Clin.*, vol. 31, no. 2, pp. 104–113, Apr. 2001.
- [13] A. Galka, O. Yamashita, T. Ozaki, R. Biscay, and P. Valdés-Sosa, "A solution to the dynamical inverse problem of EEG generation using spatiotemporal Kalman filtering," *Neuroimage*, vol. 23, no. 2, pp. 435–453, Oct. 2004.
- [14] P. Penczek, W. Grochulski, J. Grzyb, and M. Kowalczyk, "The use of a multi-channel Kalman filter algorithm in structural analysis of the epileptic EEG," *Int. J. Biomed. Comput.*, vol. 20, no. 1-2, pp. 135–151, Jan. 1987.
- [15] P. Penczek, W. Grochulski, and M. Kowalczyk, "Computer-aided analysis of the epileptic EEG," *Acta Physiol. Pol.*, vol. 37, no. 6, pp. 262–274, 1986.
- [16] S. Rump, M. Kowalczyk, and P. Penczek, "Syntactic analysis of the experimental epileptic EEG," *Pol J. Pharmacol Pharm.*, vol. 40, no. 6, pp. 585–592, 1988.
- [17] A. Schlögl, F. Lee, H. Bischof, and G. Pfurtscheller, "Characterization of four-class motor imagery EEG data for the bci-competition 2005," *J. Neural Eng.*, vol. 2, no. 4, pp. L14–L22, Dec. 2005.
- [18] P. Sykacek, S. J. Roberts, and M. Stokes, "Adaptive bci based on variational Bayesian Kalman filtering: An empirical evaluation," *IEEE Trans. Biomed. Eng.*, vol. 51, no. 5, pp. 719–727, May 2004.
- [19] M. P. Tarvainen, J. K. Hiltunen, P. O. Ranta-aho, and P. A. Karjalainen, "Estimation of nonstationary EEG with Kalman smoother approach: An application to event-related synchronization (ERS)," *IEEE Trans. Biomed. Eng.*, vol. 51, no. 3, pp. 516–524, Mar. 2004.
- [20] P. A. Valdes, J. C. Jimenez, J. Riera, R. Biscay, and T. Ozaki, "Non-linear EEG analysis based on a neural mass model," *Biol. Cybern.*, vol. 81, no. 5-6, pp. 415–424, Nov. 1999.
- [21] L. H. Zetterberg, "Recent advances in EEG data processing," *Electroencephalogr. Clin. Neurophysiol. Suppl.*, no. 34, pp. 19–36, 1978.
- [22] J.-H. Zhang, J. F. Böhme, and Y.-J. Zeng, "A nonlinear adaptive fuzzy approximator technique with its application to prediction of non-stationary EEG dynamics and estimation of single-sweep evoked potentials," *Technol. Health Care*, vol. 13, no. 1, pp. 1–21, 2005.
- [23] M. Aboy, O. W. Márquez, J. McNames, R. Hornero, T. Trong, and B. Goldstein, "Adaptive modeling and spectral estimation of nonstationary biomedical signals based on Kalman filtering," *IEEE Trans. Biomed. Eng.*, vol. 52, no. 8, pp. 1485–1489, Aug. 2005.

- [24] F. Michard, S. Boussat, D. Chemla, N. Anguel, A. Mercat, Y. Lecarpentier, C. Richard, M. R. Pinsky, and J. L. Teboul, "Relation between respiratory changes in arterial pulse pressure and fluid responsiveness in septic patients with acute circulatory failure," *Am. J. Respir. Crit. Care Med.*, vol. 162, no. 1, pp. 134–138, Jul. 2000.
- [25] F. Michard, L. Ruscio, and J. L. Teboul, "Clinical prediction of fluid responsiveness in acute circulatory failure related to sepsis," *Intensive Care Med.*, vol. 27, no. 7, p. 1238, Jul. 2001.
- [26] A. Kramer, D. Zygun, H. Hawes, P. Easton, and A. Ferland, "Pulse pressure variation predicts fluid responsiveness following coronary artery bypass surgery," *Chest*, vol. 126, no. 5, pp. 1563–1568, Nov. 2004.
- [27] F. Michard, "Changes in arterial pressure during mechanical ventilation," *Anesthesiology*, vol. 103, no. 2, pp. 419–428, Aug. 2005.
- [28] C. K. Hofer, L. Furrer, S. Matter-Ensner, M. Maloigne, R. Klaghofer, M. Genoni, and A. Zollinger, "Volumetric preload measurement by the modiolation: A comparison with transoesophageal echocardiography," *Br. J. Anaesth.*, vol. 94, no. 6, pp. 748–755, Jun. 2005.
- [29] M. Aboy, J. McNames, T. Thong, C. R. Phillips, M. S. Ellenby, and B. Goldstein, "A novel algorithm to estimate the pulse pressure variation index deltaPP," *IEEE Trans. Biomed. Eng.*, vol. 51, no. 12, pp. 2198–2203, Dec. 2004.
- [30] H. D. Portnoy and M. Chopp, "Cerebrospinal fluid pulse wave form analysis during hypercapnia and hypoxia," *Neurosurgery*, vol. 9, no. 1, pp. 14–27, Jul. 1981.
- [31] C. Contant, C. Robertson, J. Crouch, S. Gopinath, R. Narayan, and R. Grossman, "Intracranial pressure waveform indices in transient and refractory intracranial hypertension," *J. Neurosci. Meth.*, vol. 57, pp. 15–25, Mar. 1995.
- [32] B. North, "Intracranial pressure monitoring," in *Head Injury*, P. Reilly and R. Bullock, Eds. London, U.K.: Chapman & Hall, 1997, pp. 209–216.
- [33] M. Czosnyka and J. D. Pickard, "Monitoring and interpretation of intracranial pressure," *J. Neurol. Neurosurgery Psych.*, vol. 75, no. 5, pp. 813–821, Jun. 2004.
- [34] M. J. Dubin, G. Magram, and A. K. Prasad, "Intracranial pressure waveform analysis: Computation of pressure transmission and waveform shape indicators," *Neurolog. Res.*, vol. 20, pp. 533–541, Sep. 1998.
- [35] M. Chopp and H. D. Portnoy, "Systems analysis of intracranial pressure," *J. Neurosurgery*, vol. 53, pp. 516–527, Oct. 1980.
- [36] I. R. Piper, J. D. Miller, N. M. Dearden, J. R. S. Leggate, and I. Robertson, "Systems analysis of cerebrovascular pressure transmission: An observational study in head-injured patients," *J. Neurosurgery*, vol. 73, pp. 871–880, Dec. 1990.
- [37] E. L. Foltz, J. P. Blanks, and K. Yonemura, "CSF pulsatility in hydrocephalus: Respiratory effect on pulse wave slope as an indicator of intracranial compliance," *Neurological Res.*, vol. 12, no. 2, pp. 67–74, Jun. 1990.
- [38] M. Aboy, J. McNames, T. Thong, D. Tsunami, M. S. Ellenby, and B. Goldstein, "An automatic beat detection algorithm for pressure signals," *IEEE Trans. Biomed. Eng.*, vol. 52, no. 10, pp. 1662–1670, Oct. 2005.
- [39] J. Duchêne and J. Y. Hogrel, "A model of EMG generation," *IEEE Trans. Biomed. Eng.*, vol. 47, no. 2, pp. 192–201, Feb. 2000.
- [40] J. P. Kaipio and P. A. Karjalainen, "Simulation of nonstationary EEG," *Biol. Cybern.*, vol. 76, no. 5, pp. 349–356, May 1997.
- [41] M. Czosnyka, Z. Czosnyka, and J. D. Pickard, "Laboratory testing of three intracranial pressure microtransducers: Technical report," *Neurosurgery*, vol. 38, no. 1, pp. 219–224, Jan. 1996.
- [42] M. Czosnyka, Z. Czosnyka, and J. D. Pickard, "Laboratory testing of the Spiegelberg brain pressure monitor: A technical report," *J. Neurol. Neurosurg. Psych.*, vol. 63, no. 6, pp. 732–735, Dec. 1997.
- [43] R. Hornero, M. Aboy, D. Abásolo, J. McNames, and B. Goldstein, "Interpretation of approximate entropy: Analysis of intracranial pressure approximate entropy during acute intracranial hypertension," *IEEE Trans. Biomed. Eng.*, vol. 52, no. 10, pp. 1671–1680, Oct. 2005.
- [44] B. F. La Scala and R. R. Bitmead, "Design of an extended Kalman filter frequency tracker," *IEEE Trans. Signal Process.*, vol. 44, no. 3, pp. 739–742, Mar. 1996.
- [45] E. A. Wan and R. van der Merwe, "The unscented Kalman filter," in *Kalman Filtering and Neural Networks*, S. Haykin, Ed. New York: Wiley, 2001.
- [46] P. M. Djurić, J. H. Kotecha, J. Zhang, Y. Huang, T. Ghirmai, M. F. Bugallo, and J. Míguez, "Particle filtering," *IEEE Signal Process. Mag.*, vol. 20, no. 5, pp. 19–38, Sep. 2003.
- [47] G. B. Moody and R. G. Mark, "A database to support development and evaluation of intelligent intensive care monitoring," *Comput. Cardiol.*, pp. 657–660, Sep. 1996.
- [48] A. L. Goldberger, L. A. N. Amaral, L. Glass, J. M. Hausdorff, P. C. Ivanov, R. G. Mark, J. E. Mietus, G. B. Moody, C.-K. Peng, and H. E. Stanley, "Physiobank, PhysioToolkit, and PhysioNet: Components of a new research resource for complex physiologic signals," *Circulation*, vol. 101, no. 23, pp. e215–e220, Jun. 2000.
- [49] B. Goldstein, J. McNames, B. A. McDonald, M. Ellenby, S. Lai, Z. Sun, D. Krieger, and R. J. Scabassi, "Physiologic data acquisition system and database for the study of disease dynamics in the intensive care unit," *Critical Care Med.*, vol. 31, no. 2, pp. 433–441, Feb. 2003.
- [50] A. V. Oppenheim and R. W. Schaffer, *Discrete-Time Signal Processing*, 2nd ed. Upper Saddle River, NJ: Prentice-Hall, 1999.
- [51] T. L. Rusch, R. Sankar, and J. E. Scharf, "Signal processing methods for pulse oximetry," *Comput. Biol. Med.*, vol. 26, no. 2, pp. 143–159, Mar. 1996.
- [52] P. Adelson and P. Kochanek, "Head injury in children," *J. Child Neurol.*, vol. 13, no. 1, pp. 2–15, 1998.
- [53] J. F. Kraus, A. Rock, and P. Hemyari, "Brain injuries among infants, children, adolescents, and young adults," *Amer. J. Diseases Children*, vol. 144, pp. 684–691, Jun. 1990.
- [54] T. G. Luerssen, "Intracranial pressure: Current status in monitoring and management," *Seminars Pediatric Neurol.*, vol. 4, no. 3, pp. 146–155, Sep. 1997.
- [55] H. D. Portnoy, M. Chopp, C. Branch, and M. S. Shannon, "Cerebrospinal fluid pulse waveform as an indicator of cerebral autoregulation," *J. Neurosurg.*, vol. 56, no. 5, pp. 666–678, May 1982.
- [56] M. Balestreri, M. Czosnyka, L. Steiner, E. Schmidt, P. Smielewski, B. Matta, and J. Pickard, "Intracranial hypertension: What additional information can be derived from ICP waveform after head injury?," *Acta Neurochir. (Wien)*, vol. 146, no. 2, pp. 131–141, Feb. 2004.
- [57] E. R. Cardoso, J. O. Rowan, and S. Galbraith, "Analysis of the cerebrospinal fluid pulse wave in intracranial pressure," *J. Neurosurg.*, vol. 59, no. 5, pp. 817–821, 1983.
- [58] T. Ellis, J. McNames, and B. Goldstein, "Residual pulse morphology visualization and analysis in pressure signals," in *Proc. 27th Annu. Int. Conf. Eng. Med. Biol. Soc.*, Sep. 2005, pp. 2966–2969.
- [59] C. Wiesenack, C. Fiegl, A. Keyser, C. Prasser, and C. Keyl, "Assessment of fluid responsiveness in mechanically ventilated cardiac surgical patients," *Eur. J. Anaesthesiol.*, vol. 22, no. 9, pp. 658–665, Sep. 2005.
- [60] D. Austin, C. Staats, and M. Aboy, "A novel approach to pulse pressure variation estimation," in *Proc. IEEE Eng. Med. Biol. Conf.*, Sep. 2006, pp. 1391–1393.



**James McNames** (M'99–SM'03) received the B.S. degree in electrical engineering from California Polytechnic State University, San Luis Obispo, in 1992 and the M.S. and Ph.D. degrees in electrical engineering from Stanford University, Stanford, CA, in 1995 and 1999, respectively.

He has been with the Electrical and Computer Engineering Department, Portland State University, Portland, OR, since 1999, where he is currently an Associate Professor. He has published over 100 peer-reviewed journal and conference papers. His primary research interest is statistical signal processing with applications to biomedical engineering and semiconductor manufacturing. He founded the Biomedical Signal Processing (BSP) Laboratory (bsp.pdx.edu) in fall 2000. The mission of the BSP Laboratory is to advance the art and science of extracting clinically significant information from physiologic signals. Members of the BSP Laboratory primarily focus on clinical projects in which the extracted information can help physicians or medical devices make better critical decisions and improve patient outcome.



**Mateo Aboy** (M'98) was born in Pontevedra, Spain, in 1980. He received the B.S. degree (high honors) in electrical engineering and the B.S. degree (high honors) in physics with a minor in mathematics from Portland State University, Portland, in 2002, the M.S. degree (*summa cum laude*) in electrical and computer engineering from Portland State University (PSU), Portland, OR, in 2004, the M.Phil (DEA) degree from ETSIT-Vigo (University of Vigo, Vigo, Spain), where he also received the Ph.D. degree (*summa cum laude*) from the Signal Theory and Communications Department in 2005. He has completed an executive certificate in management and leadership with a focus on technical management at the Massachusetts Institute of Technology (MIT Sloan, 2007), graduate/professional coursework in IP law at the University of California, Berkeley, in 2007, and is currently pursuing the M.B.A. degree in international management at University of London, London, U.K.

He has been with the Oregon Institute of Technology (OIT), Portland, since 2005 as a tenure-track Professor in the Electrical Engineering Department. He is currently the Program Director of the Electronics program at OIT, Portland, and teaches as an Adjunct Professor in the Doctoral Program of Signal Theory and Communications at ETSIT-Vigo. He has been a research member of the Biomedical Signal Processing Laboratory (PSU) since 2000. His research is primarily focused on statistical signal processing and its applications in biomedical engineering. He has published over 50 scholarly articles and international conference proceedings papers, including 10 journal papers in the IEEE TRANSACTIONS ON BIOMEDICAL ENGINEERING.

Dr. Aboy serves as an Associate Editor and Scientific Committee Member for the IEEE-RITA Journal and President (Chair) of the IEEE Education Society in Oregon. He is a full member of The Scientific Research Society (Sigma XI), a lifetime honorary member of the Golden-Key Honor Society, a past Chapter President of HKN (International Electrical Engineering Honor Society), and past Corresponding Secretary of TBP (National Engineering Honor Society). He is a licensed Professional Engineer in Spain.